



Western

# Uncertainty Assessment of Local SAR Mapping from Radiofrequency Induced Heating of a Standardized 10.0 cm Long Titanium Rod in the ASTM Phantom at 64 and 128 MHz

Krzysztof Wawrzyn, William B. Handler, Jack Hendriks, Blaine A. Chronik  
The xMR Labs, Department of Physics and Astronomy, Western University, London ON, Canada  
Contacts: kwawrzyn@uwo.ca, bchronik@uwo.ca



## INTRODUCTION

Effects of spatial variation in transmitted RF field differ between 64 and 128 MHz [1].

Knowledge and understanding of spatial distribution is important to ensure proper testing of MR compatibility of implanted devices, especially at higher field strengths [2].

Local SAR (LSAR) can be assessed *in vitro* by direct measure of RF-induced heating of an 10.0 cm Ti rod within ASTM phantom [1].

Frequency dependant scaling factor,  $\chi$ , for rod changes temperature rise,  $\Delta T$ , to a LSAR value [1] by:

$$LSAR = \frac{\Delta T_{360s}}{\chi}$$

LSAR distribution depends on RF coil design and phantom geometry.

Meaningful implant device testing depends on knowing LSAR distribution.

A key measurement parameter is the uncertainty associated with the physical measurement process. A sensitivity factor,  $\eta$ , can be determined to quantify amount of power absorbed per mass of tissue [W/kg] per unit distance [cm].

## PURPOSE

To quantify the sensitivity factor for each directional axis due to device position dependent effects in LSAR measurements.

To support inter-laboratory and intra-laboratory comparisons.

Procedures for estimating uncertainty of measurements required by ISO/IEC 17025.

## METHODS

### Exposure System

All measurements performed on two different transmit-only body RF birdcage Medical Implant Test Systems (MITS) 1.5 and 3.0 [3], corresponding to frequencies of 64 and 128 MHz, respectively.

Table 1: MITS standard excitation sequence parameters (Software v1.12.10 [3]).

Parameters	MITS 1.5	MITS 3.0
RF Application [s]:	360	360
Pulse type:	sinc2 $\pi$	sinc2 $\pi$
Duty cycle [%]:	40	40
Pulse rep. rate [kHz]:	1.0	1.0
Polarization [°]:	270	90
Frequency [MHz]:	63.33	127.60
Power [dBm]:	59.0	60.2
Whole-body SAR [W/kg]:	2.97 $\pm$ 0.04	3.01 $\pm$ 0.18
B <sub>1,rms</sub> [ $\mu$ T]:	4.40	2.86



Figure 1: MITS 1.5/64 MHz (left) and 3.0/128 MHz (right) bench top exposure systems [3].

### Phantom

An ASTM phantom (42 x 65 x 16.5 cm) was filled with gelled Hydroxyethyl cellulose (HEC) to height of 9.0 cm [1].

HEC had electrical conductivity of 0.47 S/m  $\pm$  10 % and worst case thermal convection properties (i.e. without perfusion) of human tissue. The phantom gel was aligned with the center of the MITS.

## METHODS

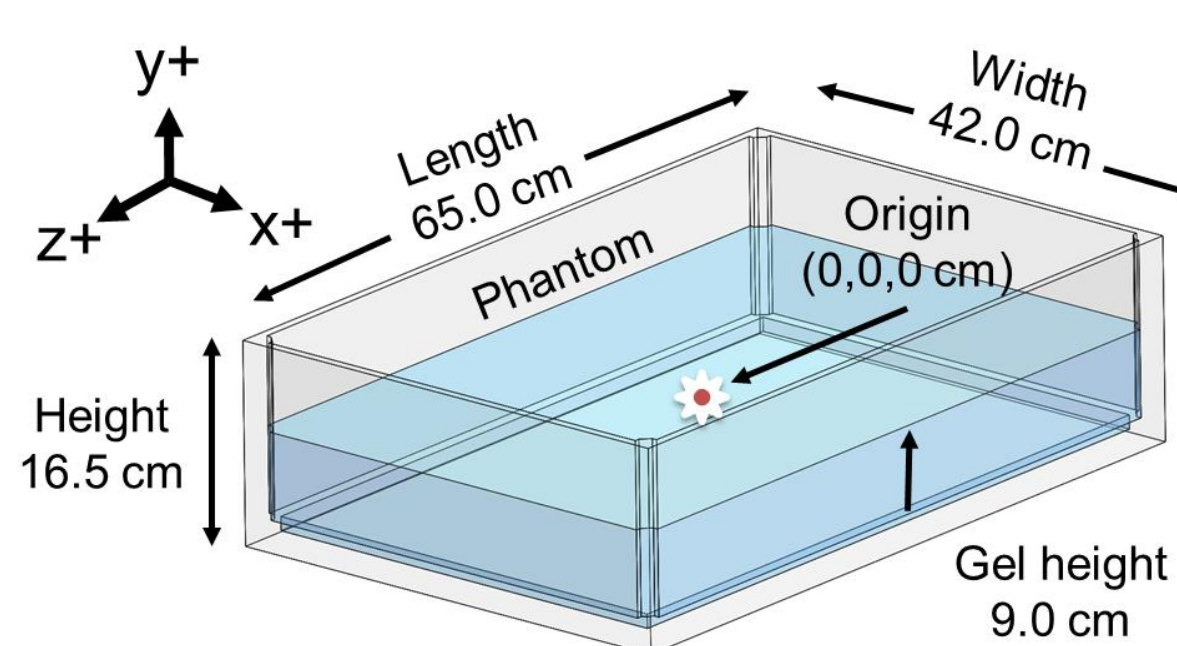


Figure 2: 3-D illustration of the phantom container filled with gelled HEC.

### Temperature Monitoring

Omniflex signal conditioner [4] with T1C optical fiber temperature probes [4] used to monitor temperature.

Normal temperature procedures were followed with acceptable temporal rates [1].

Data collection by a custom built Labview program.



Figure 3: Omniflex temperature system (left) and T1C fiber optic temperature probes (right) [4].

### Device

10.0 cm long 1/8-inch diameter Grade 5 Ti with 1.0 mm diameter holes.

Device placement is the focus and holes reduces probe placement uncertainty.

Temperature sensors [4] were placed in the holes to monitor temperature.

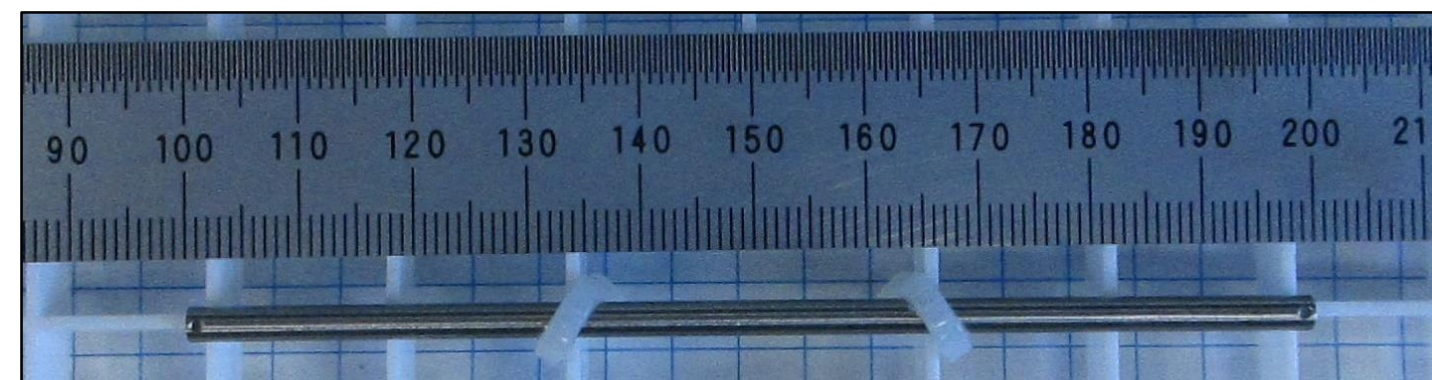


Figure 4: Photograph of 10 cm long Ti ASTM rod

### Device Positioning

Data taken at points submerged in gel, parallel to long-sided wall at different spatial increments (1-2 cm) centered on the typical implant testing location (33 mm from x-axis, 52 mm from phantom floor).

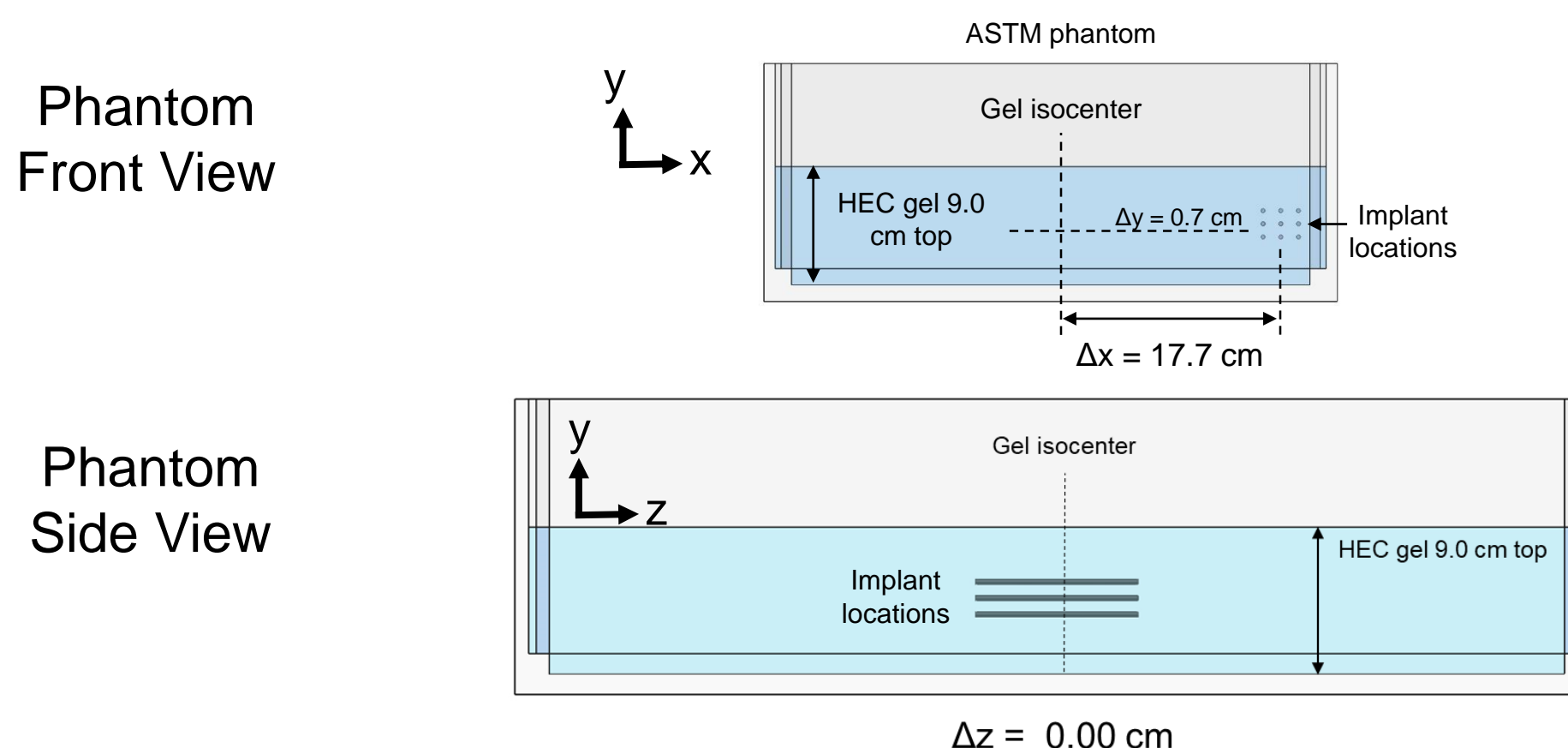


Figure 5: ASTM phantom in front view (top) and side view (bottom) with representative implant locations for 128 MHz.

### Analysis

The measured temperature change was converted to LSAR by scalar factors of 1.30 and 1.45  $^{\circ}$ C/W/kg for 64 and 128 MHz, respectively [1].

A sensitivity factor was determined for each position axis (i.e. single direction) at the central measurement locations by assuming linear dependence of the values.

## RESULTS

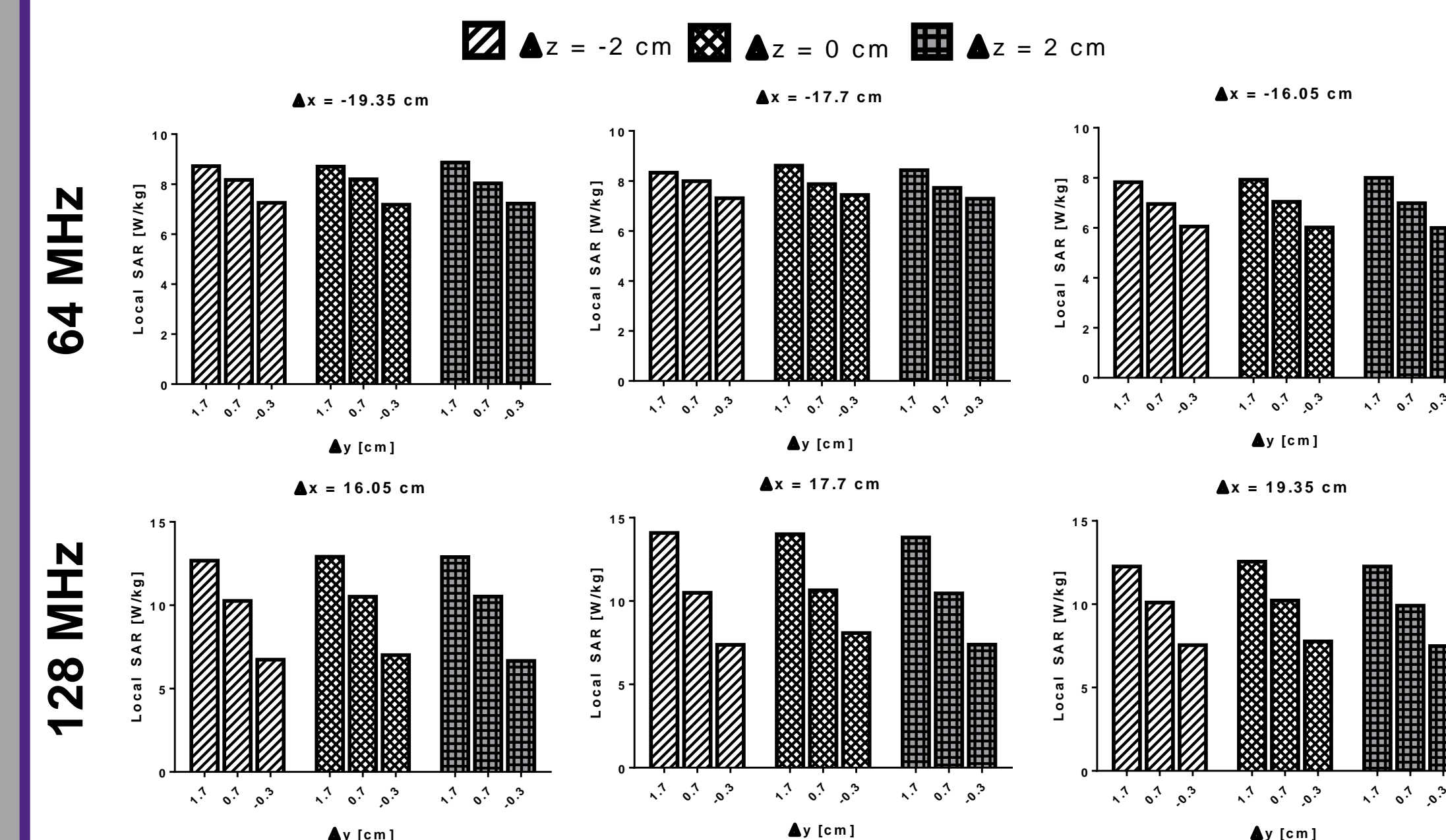


Figure 6: LSAR for different spatial locations at 64 MHz (top row) & 128 MHz (bottom row).

Sensitivity factors were determined by using central values only.

Table 2: Sensitivity factors for different directions at 64 and 128 MHz. Uncertainty determined by measurement variation in [7].

Sensitivity factor, $\eta$	64 MHz	128 MHz
$\Delta x$ [W/kg/cm]	0.29 $\pm$ 0.01	0.07 $\pm$ 0.01
$\Delta y$ [W/kg/cm]	0.59 $\pm$ 0.02	2.97 $\pm$ 0.30
$\Delta z$ [W/kg/cm]	0.10 $\pm$ 0.01	0.01 $\pm$ 0.01

## DISCUSSION AND CONCLUSION

We have quantified the extent to which the LSAR in a standardized phantom surrounding a device implant assessment location during RF testing will change with device placement was quantified.

Implant position can be one of greatest contributors to uncertainty.

Variations were greatest in implant position along y-axis as shown by sensitivity factors of 2.97 W/kg/cm (128 MHz) and 0.59 W/kg/cm (64 MHz).

As expected, variations along z- and x- axis were smaller.

This work provides additional and direct experimental quantification of the actual measurement uncertainty associated with SAR probe positioning.

These experimental findings can be used to define the contribution that device placement makes to total measurement uncertainty in device heating measurements.

Further measurements to be performed with commercial [5] and in-house [6] probes, as well as simulations to verify and validate the findings.

## ACKNOWLEDGEMENTS

The authors would like to thank Ryan Chaddock, Brian Dalrymple, and Frank Van Sas for technical support. This work was funded by NSERC Canada, Ontario Research Fund, Canadian Foundation for Innovation, and MITACS.

## REFERENCES

- [1] ASTM International F2182-11a. [2] Neufeld et al., Phys. Med. Biol. Vol. 54, pg. 4151, 2009. [3] (ZMT, Zurich, Switzerland). [4] (Neoptix, Québec, Canada). [5] (Speag, Zurich, Switzerland). [6] Attaran et al., IEEE Trans. Antennas Propag., Vol. 65, pg. 4815, 2017. [7] Wawrzyn et al., ISMRM Workshop RF Safety in MRI, Poster #20.